EINDHOVEN UNIVERSITY OF TECHNOLOGY

Hβ Stark broadening in cold plasmas with low electron densities calibrated with Thomson scattering

Citation for published version (APA):
Palomares Linares, J. M., Hubner, S., Carbone, E. A. D., Vries, de, N., Veldhuizen, van, E. M., Sola, A., Gamero, A., & Mullen, van der, J. J. A. M. (2012). Hβ Stark broadening in cold plasmas with low electron densities calibrated with Thomson scattering. *Spectrochimica Acta. Part B : Atomic Spectroscopy*, *73*, 39-47. https://doi.org/10.1016/j.sab.2012.07.005

DOI:
10.1016/j.sab.2012.07.005

Document status and date:
Published: 01/01/2012

Document Version:
Publisher's PDF, also known as Version of Record (includes final page, issue and volume numbers)

Please check the document version of this publication:

• A submitted manuscript is the version of the article upon submission and before peer-review. There can be important differences between the submitted version and the official published version of record. People interested in the research are advised to contact the author for the final version of the publication, or visit the DOI to the publisher's website.
• The final author version and the galley proof are versions of the publication after peer review.
• The final published version features the final layout of the paper including the volume, issue and page numbers.

Link to publication

General rights
Copyright and moral rights for the publications made accessible in the public portal are retained by the authors and/or other copyright owners and it is a condition of accessing publications that users recognise and abide by the legal requirements associated with these rights.

• Users may download and print one copy of any publication from the public portal for the purpose of private study or research.
• You may not further distribute the material or use it for any profit-making activity or commercial gain
• You may freely distribute the URL identifying the publication in the public portal.

If the publication is distributed under the terms of Article 25fa of the Dutch Copyright Act, indicated by the "Taverne" license above, please follow below link for the End User Agreement:

www.tue.nl/taverne

Take down policy
If you believe that this document breaches copyright please contact us at:

openaccess@tue.nl

providing details and we will investigate your claim.

Download date: 16. Nov. 2023

Spectrochimica Acta Part B 73 (2012) 39–47

Contents lists available at SciVerse ScienceDirect

Spectrochimica Acta Part B

journal homepage: www.elsevier.com/locate/sab

H_β Stark broadening in cold plasmas with low electron densities calibrated with Thomson scattering

J.M. Palomares [a,*], S. Hübner [a], E.A.D. Carbone [a], N. de Vries [a], E.M. van Veldhuizen [a], A. Sola [b], A. Gamero [b], J.J.A.M. van der Mullen [a]

[a] Department of Applied Physics, Eindhoven University of Technology, P.O. Box 513, 5600 MB Eindhoven, The Netherlands
[b] Departamento de Física, Universidad de Córdoba, Campus de Rabanales, ed. C-2, 14071 Córdoba, Spain

ARTICLE INFO

Article history:
Received 25 January 2012
Accepted 6 July 2012
Available online 16 July 2012

Keywords:
Balmer H_β
Stark broadening
Thomson scattering
Low electron density
Fine structure

ABSTRACT

In the present work Stark broadening measurements have been carried out on low electron density (n_e<5·10^{19} m^{-3}) and (relatively) low gas temperature (T_g<1100 K) argon–hydrogen plasma, under low-intermediate pressure conditions (3 mbar–40 mbar). A line fitting procedure is used to separate the effects of the different broadening mechanisms (e.g. Doppler and instrumental broadening) from the Stark broadening. A Stark broadening theory is extrapolated to lower electron density values, below its theoretical validity regime. Thomson scattering measurements are used to calibrate and validate the procedure. The results show an agreement within 20%, what validates the use of this Stark broadening method under such low density conditions. It is also found that Stark broadened profiles cannot be assumed to be purely Lorentzian. Such an assumption would lead to an underestimation of the electron density. This implies that independent information on the gas temperature is needed to find the correct values of n_e.

© 2012 Elsevier B.V. All rights reserved.

1. Introduction

Due to their wide range of working conditions, gas discharges can be used in a wide range of industrial, technological and even biomedical applications. Plasma applications can be divided among others in lighting, surface and gas treatment, and laser development [1]. In particular low temperature plasmas can offer an extended class of industrial and technological applications like surface etching, inorganic films deposition, polymerization of surfaces and sterilization [2–8].

To monitor plasma processes it is of great importance to have diagnostic tools that can provide reliable information on different plasma parameters. But in the particular case of industrial applications it is also required to have simple and easy to perform techniques that can be applied over a wide range of conditions. This study is focused on the diagnostic of one of the most important plasma parameters, the electron density n_e, in conditions of relatively low electron density (<5·10^{19} m^{-3}) and low gas temperature (<1100 K).

A very accurate technique to measure the electron density is the Thomson scattering (TS) method. This active laser technique provides precise values with spatial and temporal resolution. The method is non-intrusive provided a controlled and moderate laser power is applied. However, TS is a demanding technique that requires the use of a high power pulsed laser and a sophisticated detection setup. Therefore, TS is a diagnostic technique used in fundamental scientific research, but due to its complexity it is hardly suitable for the industrial environment. Another common method for the diagnostic of electron density is the Stark broadening technique of spectral lines spontaneously emitted by the plasma. This optical emission spectroscopy (OES) method requires a theory or model that relates the broadening of the specific used line to the values of electron density and other relevant plasma parameters like electron and gas temperatures. Although in principle this technique does not provide spatial resolution, it is a simple and reliable method.

The Stark broadening method is often applied to the lines of the hydrogen Balmer series; especially to the H_β line (486.13 nm). The broadening of this line has a strong dependence on n_e while showing a weak response on T_e. This feature makes H_β a good tool for spectroscopic diagnostic of the electron density [9–16]. A further modification of the Stark broadening technique allows determining both the electron density and temperature simultaneously by applying the Stark broadening technique to two or more Balmer lines; this is the so called Stark intersection method [17,18].

The big drawback of the Stark broadening method is that it is in principle only applicable to high n_e conditions. However, for many low temperature plasmas the electron density is well below 10^{20} m^{-3} which is lower limit of the validity region of the most commonly used Stark broadening theories [10,12,15,16]. Therefore, in order to use this technique under low density conditions, it is needed to *extend* a Stark broadening method to a lower density range. However applying such an extension we must keep in mind the reasons why the Stark theories do not reach lower densities. These mainly are the effect of the fine structure and the Doppler–Stark coupling.

* Corresponding author.
E-mail address: j.m.palomares-linares@tue.nl (J.M. Palomares).

0584-8547/$ – see front matter © 2012 Elsevier B.V. All rights reserved.
doi:10.1016/j.sab.2012.07.005

In the present study we aim to extend the Stark broadening method to low n_e and T_g conditions. To achieve this we have extrapolated the Stark tables of the numerical simulations of Gigosos et al. [15,16]. The line broadening measurements are performed with a high resolution Echelle spectrometer in order to accurately measure the line profiles. In order to deconvolute and measure the Stark broadening of the spectral line we developed a fitting code that takes other relevant broadening mechanisms into account as well as the influence of the fine structure. This method is based on the assumption that the broadening mechanism found for the H_β line as a whole can be extended to the individual fine-structure components and that Stark and Doppler broadening can be treated independently. Moreover we admit that the Stark broadening mechanism does not automatically lead to pure Lorentzian shapes.

In order to test and calibrate the extrapolation and fitting method, the measurements are performed quasi-simultaneously with TS in order to obtain precise reference values of n_e. Similarly, Rayleigh scattering (RyS) measurements are performed to obtain the values of the gas temperature. This is needed to estimate other line broadening mechanisms.

The present work is an experimental study aimed to extend a known method beyond its theoretical validity region, calibrating the results with a second independent experimental method. The extension of the Stark tables is an extrapolation of the data provided by the Stark model in its validity regime. So this semi-empirical Stark-extension method does not pretend to provide a new theory of the Stark broadening for lower density conditions.

As mentioned before, the Stark broadening of Balmer lines is a common technique for the diagnostics of the electron density. The method has been successfully applied for many years under conditions of intermediate electron densities (10^{20} m^{-3}–10^{21} m^{-3}), right above the limits of some of the Stark theories [18–20]. For low pressures and electron densities ($<<10^{20}$ m^{-3}) when Doppler broadening might be the biggest broadening mechanism, the most suitable way to measure the Stark broadening is by means of Doppler free spectroscopy [21–24]. This very precise method is used to study the Stark effect under extremely low densities. However, this is a complicated and experimentally demanding technique not suitable for the industrial practice. By means of standard OES, the Stark broadening of higher Balmer lines was already measured in [25–27] for electron densities in the order of 10^{19} m^{-3}. In [28–33] the Stark broadening of H_β line was measured at moderately low electron densities ($3\cdot10^{19}$ m^{-3}–10^{20} m^{-3}) using an extrapolation method comparable with ours, although no secondary diagnostic method was applied to check the density values obtained.

In the present study we measure the Stark broadening of the Balmer-β line in a lower density range $6\cdot10^{18}$ m^{-3}–$2.5\cdot10^{19}$ m^{-3}, and compare the results with those obtained with TS. In [34] we initially applied this method for similar conditions as a part of a study involving other diagnostic methods. However only a small density range was covered, no gas temperature measurements were included and no detailed information was given on the broadening mechanisms. In the present study we focus onto the Stark broadening method.

The present study is performed on microwave plasmas generated by a surfatron in argon hydrogen mixtures at intermediate pressures. Low temperature microwave induced plasmas, and in particular surface wave discharges, have been a subject of study within the scientific community for many years. Some common examples are the surfatron, surfaguide and waveguide surfatron [35,36]. These types of discharges can work in a wide range of pressures and gas compositions and are commonly used in several industrial applications like thin layer deposition for the production of solar cells and optical fibers [6,7]. With the surfatron used in this study we can get stable argon–hydrogen plasmas in a pressure range of 3.6 mbar–40 mbar, relatively low gas temperatures (≤1100 K) and low electron densities (≤5 10^{19} m^{-3}).

This article starts with a description of the experimental setup in Section 2. In Section 3, a short overview of the different line broadening mechanisms and their theories is presented, which is followed by the line-fitting procedure in Section 4. Results and discussion are given in Section 5, and finally Section 6 is devoted to a summary and the conclusions.

2. Experimental setup

The experimental setup can be divided into three blocks (Fig. 1): the surfatron setup; the detection branch used for the optical emission spectroscopy (OES); and the experimental setup needed to perform laser scattering measurements. The different parts have been extensively described in previous publications and only a brief description will be given here.

2.1. Surfatron

A surfatron is used to generate plasmas inside a quartz tube as discussed in [35]. The electromagnetic waves sustaining the discharge are generated by a magnetron at 2.46 GHz with a maximum power of 300 W. Coaxial cables and matching components are used to transport the microwave energy to the surfatron, in which this microwave energy is coupled into the plasma via the launching gap. The inner diameter of the quartz tube equals 6 mm, and the outer diameter 8 mm.

The plasmas are generated with argon as main gas. The pressure ranges from 3.6 mbar up to 40 mbar, while the input microwave power is kept constant at 60 W. To obtain a measurable intensity of the H_β line, it was necessary to add small amounts of molecular hydrogen to the plasma. The percentage of H_2 admixed with Ar ranges from 1% to 3%. Changing the pressure and H_2 concentration in the mentioned ranges we obtain 8 different plasma conditions. For each condition the H_β is measured with the OES branch while a reference TS measurement is taken with the laser scattering setup. In Table 1 we present all the experimental conditions ordered by increasing electron density (measured with TS).

It may be noticed that for a fixed H_2 concentration the electron density does not always increase with pressure as it would be expected [37]. The reason is that although the applied microwave power is constant, the quality of the energy coupling between launcher and plasma may change for each condition. This leads to different lengths of the generated plasma columns, but the measurements are taken at a fixed position from the launcher and not from the end of the column. As a consequence the density results do not follow a coherent trend. However, as stated before the aim is to compare Stark and TS results for different density conditions, and not to study the behavior of the surfatron plasma.

2.2. Optical emission spectroscopy detection branch

The plasma light was focused by a quartz lens in the direction transversal to the surfatron tube axis onto an optical fiber. The lens has a diameter of 5 mm and a focal length of 10 mm; the core diameter of the fiber is 200 μm (Fig. 1). Between the lens and the plasma a set of two 1 mm pinholes is placed with 20 cm distance from each other. The combination of lens and pinholes forms a collimator. In this way only the light emitted along a single line of sight through the diameter of the quartz tube is collected (Fig. 2). With this configuration the spectroscopic measurements represent an average value over the tube diameter. All the measurements were taken at a fixed axial position of 4 cm after the launcher gap.

The fiber then guides the collected light to a high resolution spectrometer, called the Double Echelle MONochromator, abbreviated to DEMON [38]. The DEMON consists of a prism pre-monochromator in sequence with a high resolution CCD Echelle spectrometer. The

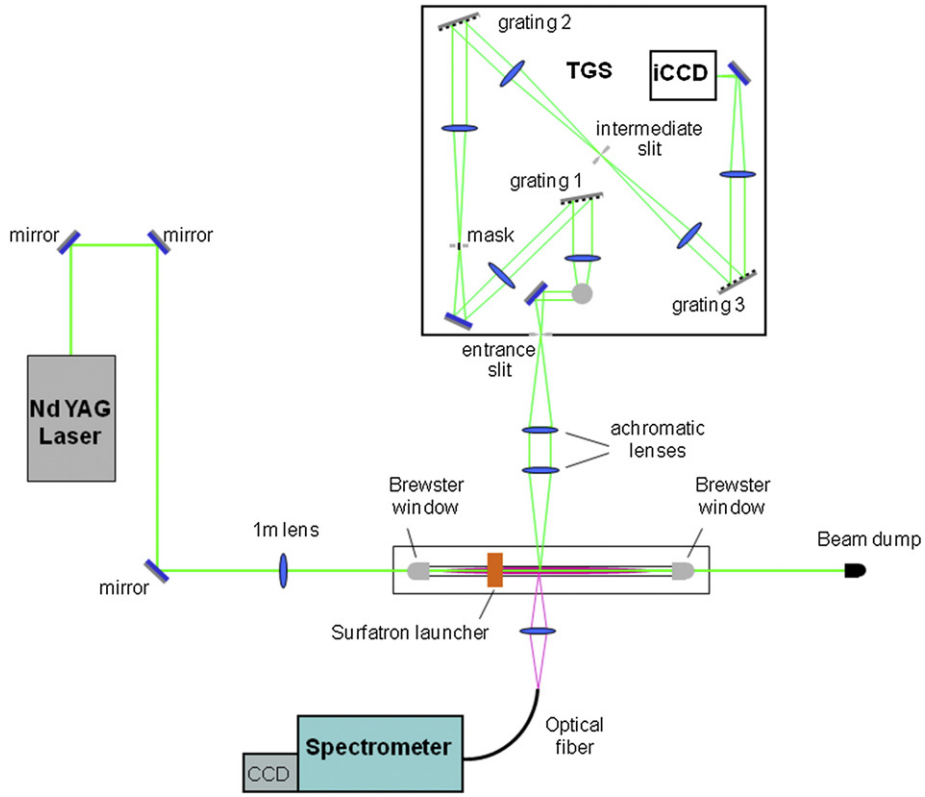

Fig. 1. Schematics of the experimental setup. Three main parts can be distinguished. The plasma source or surfatron; the optical emission spectroscopy (OES) detection branch; the laser scattering setup composed by the Nd:YAG laser and the active detection branch using a triple grating spectrograph (TGS).

prism pre-monochromator is used for the separation of the different spectral orders formed by the grating. The Echelle monochromator is the high resolution component of the spectrometer. In this configuration, internal order separation and high resolution are received. To record the spectrum, an Andor DV434 CCD was used. The 1024 × 1024 array consists of pixels with a size of 13 × 13 μm. Thermoelectric cooling results in a negligible dark current.

2.3. Laser scattering setup

The setup used to perform TS experiments is exactly the same as that shown in [37]. In Fig. 1 the main components are shown. A Nd:YAG laser working on the second harmonic at $\lambda = 532$ nm generates 100 mJ pulses with a repetition rate of 10 Hz. These are directed along the central axis of the plasma tube. The scattering signal is collected with two achromatic lenses and focused onto the entrance of a triple grating spectrometer (TGS). The TGS is designed to collect the Thomson signal while removing the Rayleigh and false stray light photons in the central part of the spectrum [39]. The same setup without the filtering function is used to perform RyS measurements and to obtain the gas temperature [40]. The scattering measurements are all taken at the same axial position as the spectroscopic ones; i.e. at 4 cm after the launcher gap.

As explained in the references above [37,39], the laser is aligned along the surfatron axis exactly in the center of the quartz tube. Therefore we obtain values of n_e and T_g (measured respectively with TS and RyS) at the radial center of the tube (Fig. 2). This stands in contrast to the OES measurements that deliver line of sight averaged values along the tube diameter. In order to compare the results of the different techniques we assume a Bessel profile of n_e along the radius [41]. Then it is possible to calculate the n_e averaged value over the tube diameter from the TS results at the central position. The TS scattering results presented here are already averaged over the diameter so that they can directly be compared with the Stark broadening results. For the values of T_g we assume a constant radial profile.

Table 1
Experimental settings and n_e and T_g values obtained with TS and RyS respectively. The applied microwave power was 60 W for every case. All measurements were taken at an axial distance of 4 cm from the launcher gap.

Condition	Pressure (mbar)	H_2 concentration	n_e (m^{-3}) (TS)	T_g (K) (RyS)
1	40.6	1%	$6.73 \cdot 10^{18}$	1100
2	10.2	3%	$8.88 \cdot 10^{18}$	1100
3	9.4	3%	$8.93 \cdot 10^{18}$	1100
4	3.6	3%	$1.04 \cdot 10^{19}$	600
5	14.7	3%	$1.16 \cdot 10^{19}$	1100
6	5	1%	$1.54 \cdot 10^{19}$	500
7	10.3	1%	$2.03 \cdot 10^{19}$	750
8	20.3	1%	$2.46 \cdot 10^{19}$	1000

3. Broadening of spectral lines

The shape of a spectral line contains information of fundamental plasma quantities. The principal broadening mechanisms are: natural broadening, Doppler broadening, pressure broadening and Stark broadening. In addition, a spectral line will be broadened by the apparatus profile of the spectrometer. Also the fine structure has to be considered. In this section, the various broadening mechanisms are discussed and their contributions to the total line broadening are estimated for typical plasma conditions.

3.1. Natural and resonance broadening

Natural broadening is caused by the finite lifetime of excited states and can be determined from the Heisenberg uncertainty relation; $\Delta E \cdot \Delta\tau \geq h/2\pi$. The lifetime τ_p of state p due to spontaneous emission is called the natural lifetime. Using the Heisenberg relation, it is

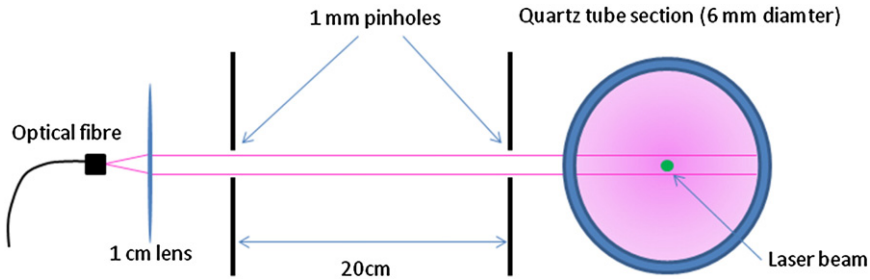

Fig. 2. Diagram of the light collection setup for the optical emission measurements. Thanks to the collimation only light emitted along the tube diameter is collected.

possible to calculate the full-width at half-maximum (FWHM) due to the natural broadening, $\Delta\lambda_{nat}$. For H_β, the natural broadening is ~10^{-3} pm. As we will see this is much smaller than other broadening mechanisms and can therefore be neglected.

Resonance broadening is caused by collisions of radiating hydrogen atoms with other hydrogen atoms of the same species. For the case of H_β, a pressure of 10 mbar and a concentration of hydrogen of 1%, the resonance broadening is ~10^{-2} pm [42,43]. This is 10 times larger than the natural line width, but as we will show, this value is also negligible for our plasma conditions.

3.2. van der Waals broadening

van der Waals broadening is caused by the presence of atoms of a different kind than those of the emitting hydrogen particle. The induced dipole of the ground state argon atoms interacts with the emitting hydrogen atom which results in a Lorentzian broadening of the spectral line. In [44] a general description of the van der Waals broadening for non-hydrogenic lines is given. In the work of Yubero et al. [45], the van der Waals broadening is determined for emitting hydrogen atoms in atmospheric argon plasmas for the first three lines of the hydrogen Balmer series. As the van der Waals broadening is proportional to the pressure, we can scale these expressions to a lower pressure. This gives the following expression for the H_β FWHM

$$\Delta\lambda_w = \frac{5.521}{T_h{}^{7/10}} p \tag{1}$$

where $\Delta\lambda_W$ is the van der Waals FWHM expressed in nm, T_h the heavy particle temperature in K and p the pressure in bar. This broadening term depends solely on the gas temperature and gas pressure.

For typical conditions of $p \sim 10^{-2}$ bar and $T_h \sim 800$ K, a width of 0.5 pm is obtained. As we will see, this value is relatively small compared to the Stark and Doppler widths and the correction introduces only a minor decrease in the results. Nevertheless, this correction will be taken into account in our calculations.

3.3. Doppler broadening

Doppler broadening is caused by the velocity distribution of the emitting particles. The intensity distribution of a Doppler-broadened spectral line has a Gaussian shape of which the full-width $\Delta\lambda_D$ equals

$$\Delta\lambda_D = 7.16 \times 10^{-7} \lambda_0 \sqrt{T/A} \tag{2}$$

where A is the atomic mass of the emitter expressed in a.m.u., T the temperature of the emitting species in K and λ_0 the central wavelength of the spectral line in nm. Using this formula, a Doppler temperature can be obtained from the Gaussian part of a spectral line. Inserting a typical atom temperature of ~800 K into Eq. (2) results in a Doppler width (FWHM) of $\Delta\lambda_D \sim 10$ pm.

As it will be seen later, under our plasma conditions the Doppler broadening is in the same order as the instrumental and Stark widths. As it was stated in the introduction, the aim is to measure the Stark broadening and therefore it is of great importance to have good estimations of T_g in order to precisely obtain the Doppler widths.

3.4. Stark broadening

Various Stark broadening theories have been developed and refined in the past. These theories range from the model of quasi-instantaneous electron collisions of Lorentz (or impact model) [9], via the quasi-static theories for ion collisions [10–12], to finally reach the recent micro-field model methods (MMM) [13,14]. An extensive historical review can be found in [46]. The different theories provide expressions to calculate the Stark broadening as a function of the electron density and temperature. Classical examples are the theories of Vidal, Copper and Smith (VCS) or Kepple and Greim (KG) [11,12]. One of the most refined Stark broadening theories was developed by Gigosos and Cardeñoso [15,16] (GC) using computer simulations. The main advantage of the GC model is the consideration of ion dynamics and the possibility of working with two temperature plasmas. For these reasons the computer simulations of GC have been chosen as the Stark broadening model for the diagnostics of the electron density in this work. However, it must be said that all the mentioned theories are derived for n_e values above 10^{20} m^{-3}. Consequently none of them can be expected to be theoretically valid for lower densities.

The GC model calculates the theoretical line profiles of H_α, H_β and H_γ for a T_e-range of 10^3 K–10^6 K, a n_e-range of 10^{20} m^{-3}–10^{25} m^{-3} and a range of the relative reduced mass of 0.5–10. This relative reduced mass is defined by $\mu_r = (T_e/T_h)\mu$, where μ is the reduced mass of the colliding system. For argon plasmas with small amounts of hydrogen, the reduced mass is close to unity so that μ_r equals the ratio of electron and heavy particle temperatures, T_e/T_h. Via μ_r the GC model can account for non-thermal equilibrium conditions. This is important since the low pressure microwave induced plasmas are not in thermal equilibrium ($T_e > T_h$).

Using the GC model for the Balmer H_β line, the full-width at half-maximum (FWHM) or $\Delta\lambda_S$ is given in terms of T_e, n_e and μ_r. Fig. 3 shows the dependence of FWHM with n_e for the case of $T_e =$ 15,000 K and $\mu_r = 10$ according to the GC tables [15,16]. It can be seen that the GC model gives a linear relationship between $\log(\Delta\lambda_S)$ and $\log(n_e)$. With the use of such a linear fit we can extrapolate the GC tables to obtain the values of $\log(\Delta\lambda_S)$ for electron densities in the order of 10^{19} m^{-3}. For $n_e = 10^{19}$ m^{-3} the extrapolation of Fig. 3 leads to a Stark width of 9.5 pm.

Other spectroscopic studies [28–31] also used extrapolations of H_β Stark broadening tables beyond their theoretical validity region, but not to such low n_e-values. Moreover the results were not compared with other techniques. In [28] the authors used a similar linear fit of the GC tables, although for higher values of electron densities. In [29–31] the Stark tables of Griem were extrapolated to electron densities in the order of 5 10^{19} m^{-3}.

As previously remarked, typical conditions for our plasmas are $T_e \sim 15{,}000$ K and $T_h \sim 1000$ K, which implies a value of the relative reduced mass of $\mu_r \sim 15$. Since the GC tables only provide values of μ_r up

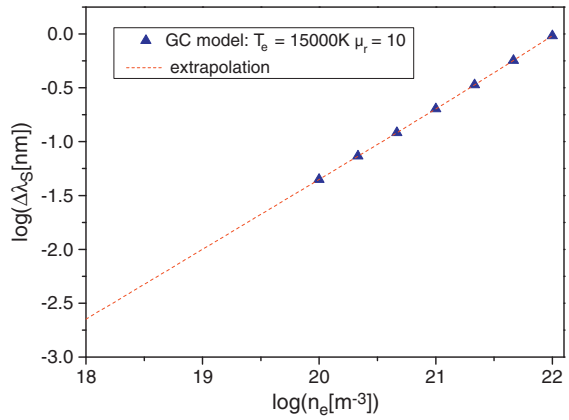

Fig. 3. Calculated values of Stark width, $\Delta\lambda_S$, with the GC model for the conditions of $T_e = 15{,}000$ K, $\mu_r = 10$. The red dashed line represents the extrapolation of the table to lower electron densities.

to 10, we will use the tables of GC for the case of $T_e = 15{,}000$ K and $\mu_r = 10$ (Fig. 3). Nevertheless it can be deduced from the GC tables that the influence of μ_r is very small for low densities. Extrapolating the tables for different values of μ_r gives an estimation of the error in this parameter lower than 1%.

In the following discussion it is useful to distinguish between the line shapes and the underlying mechanisms; this in fact is a distinction between mathematics and physics. A broadening mechanism is the result of a physical effect that changes the shape of a spectral line. Some broadening mechanisms like Doppler broadening may be described with a basic shape like Gaussian, but this is not the case for the Stark broadening. In the first Stark broadening theories [9] it is calculated to have pure Lorentzian line shapes. However the line profiles obtained in the GC numerical simulations are clearly non-Lorentzian. Still there are several studies in which pure Lorentz shapes are adopted for the Stark broadening [28–32]. We will show in Section 5 that assuming a perfect Lorentzian shape for the Stark profiles leads to an underestimation of the electron density and consequently to an overestimation of the gas temperature. In principle we do not assign any basic shape to the Stark broadening.

In the procedure we fit the experimental lines to a Voigt curve modified by the fine structure. Being more flexible than Lorentzian or Gaussian type, a Voigt curve fits more accurately the experimentally measured lines. Simultaneously, the use of Voigt curve allows removing other broadening mechanisms (i.e. Doppler, van der Waals, instrumental) that are described by basic shapes (i.e. Gaussian, Lorentzian). Consequently, after removing all the other broadening mechanisms also a Voigt profile remains. The FWHM of this remaining Voigt curve is taken as the Stark width, $\Delta\lambda_S$, and together with the extrapolated tables it provides the estimated value of the electron density. However, we should keep in mind that using a Voigt shape for a Stark broadened line is an approximation.

Another important topic is that of the possible change in the nature of Stark broadening that takes place for decreasing electron densities. It is well known that for electron densities higher than 10^{20} m^{-3} the Stark width scales as $\Delta\lambda_S \sim n_e^{2/3}$. However, for very low n_e values, e.g. in the order of 10^{16} m^{-3} the Stark width of a single fine structure component as studied by Doppler free spectroscopy was found to be linear with density, $\Delta\lambda_S \sim n_e$ [22,47]. So, an important question is whether the nature of the Stark broadening mechanism changes during our extrapolation towards low n_e values. In [48] numerical simulations were carried out for the Stark width of single fine structure components of the three first Balmer lines. The authors found that the approximation of $\Delta\lambda_S \sim n_e^{2/3}$ holds for H_β until an electron density of 2 10^{18} m^{-3}. This is below our n_e range of interest. In the next sections we will deal with other effects that can play a role in the line width like the effect of the Doppler coupling and the shifting of the fine structure components. But from the point of view of the extrapolation, the results shown in [48] indicate that the extrapolation is still valid for the Stark width of a single component in our range of electron densities.

3.5. Doppler–Stark coupling and fine structure

There are two main reasons why the common Stark theories are not calculated for low electron densities: the *coupling* between Doppler and Stark broadening and the effect of the *fine structure*. We recall that this is an experimental study and that we do not intend to give an ab initio theoretical derivation of the Stark broadening mechanism at low electron densities. We simply extrapolate a theory valid at higher densities to a low density regime and calibrate the results with an independent experimental technique. Nevertheless, in this section we address the two effects since they must be kept in mind.

At high electron densities ($>10^{20}$ m^{-3}) when the Stark broadening is dominant over the Doppler broadening both effects can be considered statistically independent. In this situation the Doppler contribution can be simply convoluted with the Stark profile. On the other hand, when Doppler is comparable or more important than Stark the two effects are correlated and both mechanisms must be calculated simultaneously. In [49] the Doppler and Stark broadenings are calculated simultaneously for the Lyman-β line with electron densities in the order 10^{21} m^{-3} and a gas temperature of 12,000 K. It was found that under such high densities the results of the calculations with Doppler–Stark coupling do not differ from a simple Doppler–Stark convolution. As shown before the values of Stark and Doppler broadenings are comparable under our plasma conditions. Still, we work under the estimation that Doppler and Stark are independent and that they can be convoluted to create the final line profile.

However the main factor that limits the common Stark theories is the presence of a fine structure. The H_β spectral line consists of a series of components or individual transitions spectrally positioned at small distances from each other. They originate from transitions between the sublevels of the upper level with principal quantum number n = 4 to the lower level with n = 2. In the GC model as well as in the theories mentioned in Section 3.4, only one line component is considered. This assumption is valid when the total line broadening is much wider than the separation between the fine structure components. At lower electron densities this problem is not easy to deal with because the fine structure splitting and the intensity of components might change with the electric plasma micro field [21–23,50]. Some preliminary calculations of Stark profiles on hydrogen lines with fine structure effect were done for the H_α line in [51]. Recently more complete calculations have been performed in [27,48,52], however there are still no complete tables of Stark broadening for the first Balmer lines including the fine structure effect. In [48] it is estimated that for the case of H_β there is no need to introduce the fine structure for densities above $4 \cdot 10^{19}$ m^{-3}. Our range of densities is right below the mentioned limit and therefore we must account for this effect. As an estimation we use the fine structure under conditions of zero electric field [53], of which the main parameters are presented in Table 2. The final line profile used for the fitting of the experimental results is composed from the convolution of all the broadening mechanisms described in Section 3 with each of the fine structure components of Table 2.

3.6. Instrumental broadening

The optical system used to record the spectrum causes an extra broadening of spectral lines. This type of broadening is called *instrumental broadening* and is independent of the plasma properties (instrumental function). It is determined by parameters of the

Table 2
The fine structure components of H_β.

n = 4	n = 2	λ (nm)	A_j (10^6 s^{-1})	g_j	$I_{relative} = g_jA_j/\sum g_iA_i$
$^2D_{3/2}$	$^2P_{1/2}$	486.1279	17.18	4	0.26
$^2P_{3/2}$	$^2S_{1/2}$	486.1287	9.668	4	0.14
$^2S_{1/2}$	$^2P_{1/2}$	486.1288	0.8593	2	0.01
$^2P_{1/2}$	$^2S_{1/2}$	486.1298	9.668	2	0.07
$^2D_{5/2}$	$^2P_{3/2}$	486.1361	20.62	6	0.46
$^2D_{3/2}$	$^2P_{3/2}$	486.1365	3.437	4	0.05
$^2S_{1/2}$	$^2P_{3/2}$	486.1375	1.719	2	0.01

spectrometer like the width of the entrance slit, the type of grating, the focal length and the sensor.

The FWHM of the DEMON is specified to be 6.1 pm at a wavelength of 486 nm [38]. However, we checked the instrumental profile by measuring an argon line under conditions for which all broadening effects are much smaller than the instrumental one. A good candidate is the argon spectral line at a wavelength of 470.23 nm, that is intense enough to be measured with a good signal to noise ratio and it is close to the wavelength of H_β.

For the measurement of this argon line, an argon plasma was made at low pressure ($p = 0.5$ mbar) and low power (≈ 15 W), and the measurement was performed far away from the launching gap. Under this condition, the gas temperature is estimated to remain below 350 K [40] and the electron density below $5 \cdot 10^{18}$ m^{-3}. Using Eq. (2) with $A = 40$ a.m.u. and $\lambda_0 = 470.23$ nm results in a Doppler broadening of $\Delta\lambda_D = 0.9$ pm. For an electron density of $5 \cdot 10^{18}$ m^{-3}, it can be calculated with the Griem theory [12] that the Stark broadening of this argon line is <0.1 pm. Using the general description of [44] it is found that the van der Waals broadening is in the order of ~0.01 pm. Therefore the Stark and van der Waals broadenings are negligible for this argon line. After the Doppler contribution is subtracted, a new Gaussian profile is left with only the instrumental contribution. This Gaussian instrumental profile has a FWHM of 5.9 pm that is in very good agreement with the technical specifications of the DEMON and will be used to correct any experimental line broadening for this contribution.

4. Fitting procedure

As discussed before the Stark broadening does, in general, not lead to a standard profile such as a Lorentzian (or Gaussian). As a consequence we cannot separate the experimental line profiles in a composition of basic shapes, each of them corresponding to separate broadening mechanism. Thus we have to break with the practice often found in literature that after deconvolution the Gaussian component is automatically attributed to Doppler (T_g) and the Lorentzian to the Stark (n_e). This implies that we can only obtain the magnitude of the Stark broadening after calculating and removing every other mechanism. With this procedure our fitting code leads to a Voigt curve describing the Stark broadening in an approximate way.

As shown in Section 3 there are different broadening mechanisms with a non-negligible contribution to the composed line profile, and therefore a fitting procedure is needed to deconvolute them. The procedure is divided in four steps:

I. *Corrected instrumental profile*. First, the instrumental profile is convoluted with the fine structure forming the corrected instrumental profile.
II. *Calculated profile*. The profile is convoluted with a variable Voigt curve forming the calculated complete profile.
III. *Fitting*. The variable Voigt of the calculated profile is then changed until the best fit is obtained with the experimentally measured H_β line.
IV. *Stark broadening*. Finally, from the fitted Voigt we can obtain the Stark broadening after removing the contributions of the other mechanisms.

4.1. Corrected instrumental profile

The Gaussian instrumental profile is determined as explained in Section 3.6. To correct for the influence of the fine structure, which was presented in Table 2, a convolution of this instrumental profile with the fine structure has to be performed.

The instrumental profile is presented by a dashed red line on Fig. 4. The fine structure of H_β, is shown as a set of green vertical dotted lines. Finally the solid black line, referred to as corrected instrumental profile, is the result of the convolution of the instrumental profile and the fine structure. This corrected instrumental profile is independent of the plasma properties.

4.2. Calculated profile

The second step is to introduce the contributions of the other broadening mechanisms, mainly Stark and Doppler broadening, and in a lower degree van der Waals. A variable Voigt curve is used to represent the combined effect of all this broadening mechanisms, although at this point no calculation is made on any of them. In the fitting code this Voigt curve is convoluted with the corrected instrumental profile, generating the so called calculated profile.

4.3. Fitting

This calculated profile is now compared with the measured H_β line profile. Using a least squares fitting procedure, the Gaussian and Lorentzian widths of the variable Voigt curve are varied until the best fit is obtained. An example of one of the measurements, its theoretical fit and the fit-residue are shown in Fig. 5. Although it is a small detail, the calculated profile results in an asymmetrical line. Since the instrumental profile is symmetric, this asymmetry is the result of the fine structure.

4.4. Stark broadening

The Voigt curve obtained from the fitting contains only the contributions of the Stark, Doppler and van der Waals broadening, since the instrumental broadening and the fine structure are already accounted for in the corrected instrumental profile. With the help of Rayleigh scattering measurements (Section 2.3) gas temperature values are obtained for each plasma condition. With these values and Eqs. (1) and (2) the Lorentz–van der Waals and Gauss–Doppler contributions are calculated. Then the Doppler width is removed from the Gaussian part of the fitted Voigt and the van der Waals width from the

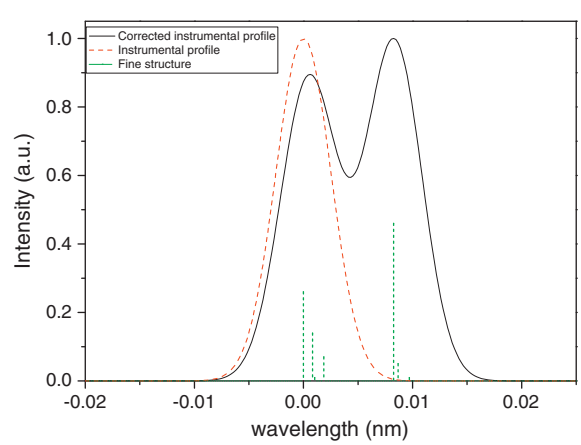

Fig. 4. Instrumental profile (red dashed line), fine structure (green vertical dotted lines) and the convolution of both: the corrected instrumental profile (solid black line).

Lorentzian part. The remaining profile is another Voigt curve that represents only the Stark contribution. The FWHM of this Voigt curve is then used as the Stark width, $\Delta\lambda_S$, and together with the extrapolated tables from GC model (Section 3.4) provides the measured values of electron density, n_e.

As stated in Section 3, it is often assumed that Stark profiles are purely Lorentzian. Under this assumption both T_g and n_e can, in theory, simultaneously be obtained from the line fitting. Under this erroneous assumption the whole Gaussian component of the fitted Voigt is completely attributed to the Doppler broadening. Then, with Eq. (2) the value of T_g is obtained. Similarly the Lorentz component of the fitted Voigt (minus the van der Waals contribution) is seen as the Stark contribution and used to derive n_e. We will show in Section 5 that this assumption leads to a systematic overestimation of the gas temperature and an underestimation of the electron density.

5. Results and discussion

In the left graph of Fig. 6 we present the values of electron densities obtained from the Stark broadening for the 8 different plasma conditions (Table 1). The broadening results are compared with those obtained by Thomson scattering for the same experimental conditions. The conditions cover a range in electron density of $6\cdot10^{18}$ m^{-3}–$2.5\cdot10^{19}$ m^{-3}. The Stark fitting results show a similar trend as the TS results, with an average relative deviation of 20% from the TS measurements. This reasonable agreement validates the extrapolation of the GC tables and fitting method as a tool for the estimation of n_e, at intermediate-low density conditions.

In the right graph of Fig. 6 we present the same experimental results but this time compared with the extrapolation of the used GC Stark tables (Fig. 3). The experimental points shown in the figure are obtained combining the n_e values measured with TS and the Stark widths ($\Delta\lambda_S$) measured with the fitting procedure. Although the results of left and right graphs are somehow redundant, the latter shows the validity of the extrapolation procedure. As discussed in Section 3.4, this graph proves that the Stark broadening of a single fine structure component scales with $\Delta\lambda_S \sim n_e^{2/3}$ until electron densities in the order ~5 10^{18} m^{-3}.

The estimation of the errors in the present measurements can only be done partially. As explained in Section 3.4, the computer simulations of GC provide the Stark broadening for different values of n_e, T_e and μ_r. Using the tables for different values of T_e and μ_r one can estimate the errors introduced due to the uncertainties of these parameters. Assuming errors of ±5000 K in T_e and ±5 in μ_r we find a relative error in n_e of 4% for densities around 10^{19} m^{-3}, which can be seen as a modest error. On the other hand the gas temperature has a much greater influence. In order to have reliable results it is of crucial importance to have precise values of T_g. In our particular case we determine the relative errors in T_g obtained with RyS to be in the order or below 20%. This leads to an error in n_e of ~20%, what is in agreement with the deviation measured with respect to the TS results.

However, as explained in Sections 3.4 and 3.5, the Stark tables used are designed for electron densities above 10^{20} m^{-3}. The theoretical error that the extrapolation carries cannot be calculated with the present results.

Finally in Fig. 7 we present results assuming a purely Lorentzian Stark profile. As explained in Section 4, under this assumption both n_e and T_g can be obtained from the fitting of the line profile. In the left graph of Fig. 7 the density results are compared with TS, while in the right graph the gas temperature results are compared with RyS. The n_e results are systematically underestimated by about 50% while simultaneously the T_g values are overestimated by about 70%. This strict separation of Gauss = Doppler and Lorentz = Stark has led to many discrepancies. For instance in [32] a Lorentz profile was assumed for the Stark broadening. The density results were not compared with any other technique, but the obtained temperatures from the H_β broadening were almost 100% higher than the OH rotational temperature.

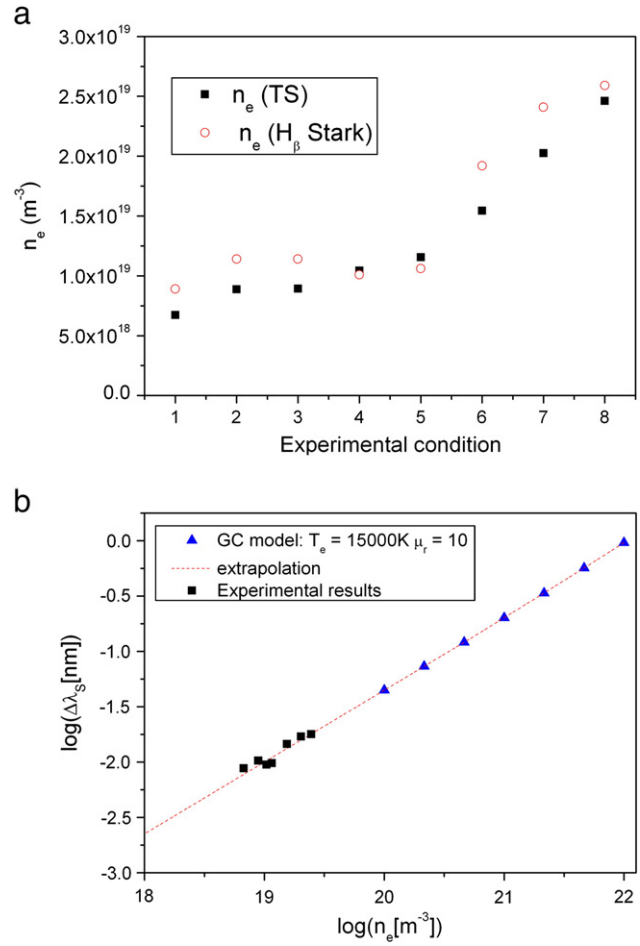

Fig. 6. Experimental results of n_e for all the plasma conditions. Left graph compares the Stark broadening results (empty red circles) with the TS measurements (solid black squares). Right graph compares the extrapolation of the GC tables at $T_e = 15{,}000$ K, $\mu_r = 10$ (Fig. 3) with the experimental points: $\Delta\lambda_S$ (fitting) – n_e(TS).

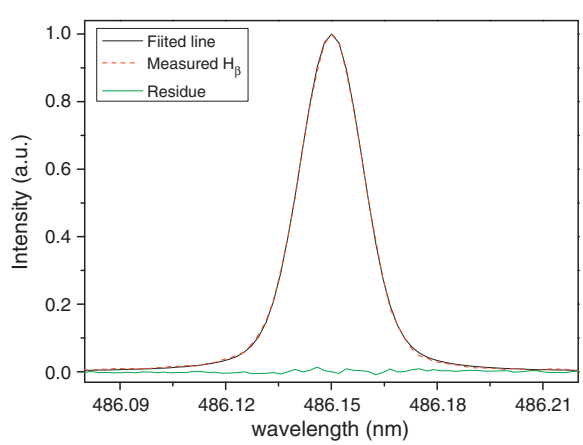

Fig. 5. Results of the fitting code on the H_β profile measured at experimental condition 1. Dashed red line: measured profile; solid black line: fitted line generated with the fitting code; solid green line: residue between the fitted and measured lines.

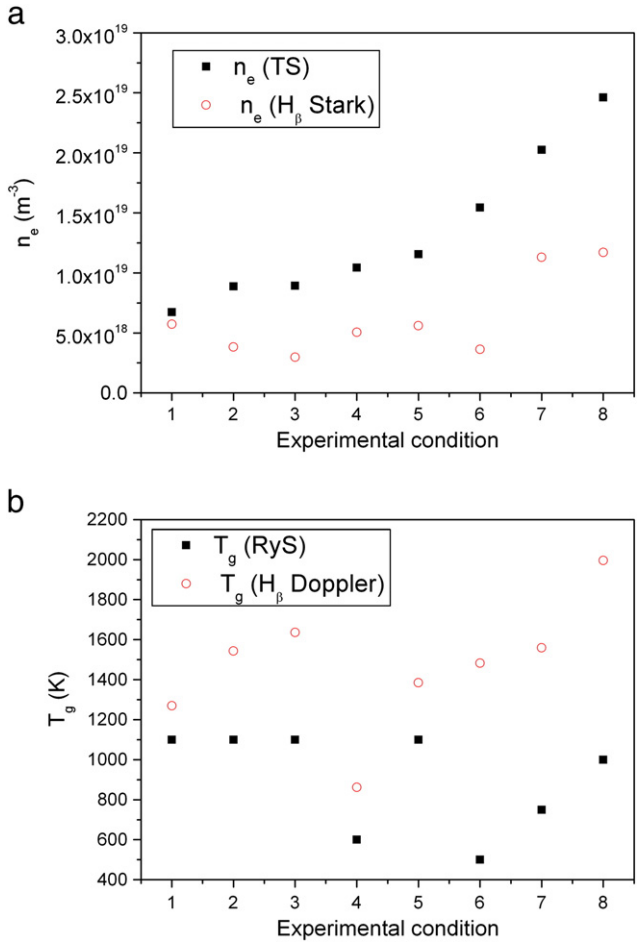

Fig. 7. Results assuming a Lorentzian curve for the Stark broadening. Left graph compares the n_e results obtained with the H_β line Stark broadening and TS. Right graph compares the T_g results obtained with the H_β line Doppler broadening and RyS.

The results shown in Fig. 7 indicate that at such low densities a basic Lorentzian line shape cannot be assumed for the Stark profile. But this implies that we cannot obtain simultaneously T_g and n_e from line broadening measurements. In other words, since there are no Stark tables at low densities that provide full Stark profiles, it is not possible to fit two parameters from the spectral line shape. One of them must be estimated independently and introduced in the fitting process.

6. Summary and conclusions

In the present study we have used the Stark broadening of the H_β spectral line to determine the electron density of low temperature and low density argon–hydrogen plasmas, under intermediate-low pressure conditions. To do so, a line fitting code is used to separate other broadening mechanisms, mainly the Doppler and instrumental contribution from the line width. The line measurements are performed with a standard optical emission spectroscopy setup and a high resolution spectrometer. In order to obtain the electron density values from the Stark-width we use the Stark tables obtained with the computer simulations of Gigosos et al. The results are then compared with those obtained with Thomson scattering measurements performed under the same plasma conditions.

However, the density range covered in our experiment ($6\cdot10^{18}$–$2.5\cdot10^{19}$ m^{-3}) is below the limit of the GC model. An extrapolation to lower densities is needed. In order to do that the fine structure of the line is introduced externally. Although the extrapolation is not supported by an ab initio calculation, the results show a good agreement between the 20% with the precise values of the TS technique. This agreement validates the use of the Stark broadening at low n_e conditions with simple optical emission spectroscopy.

It is also pointed out that the method needs precise values of the gas temperatures by an independent technique. The precision of the electron density results is directly linked to those of the gas temperature. Similarly, it is found that Stark broadening does not lead to pure Lorentzian shapes. This implies that T_g and n_e cannot be deduced simultaneously from the Stark profile. Doing so causes systematic overestimations of the gas temperature and underestimations of the electron density.

Acknowledgments

This work is supported and financed by the Dutch Technology Foundation STW under the project numbers 10744 and 10497 and the bilateral relation between the University in Eindhoven (the Netherlands) and Cordoba (Spain).

References

[1] A. Bogaerts, E. Neyts, R. Gijbels, J.J.A.M. van der Mullen, Gas discharge plasmas and their applications, Spectrochim. Acta Part B 57 (2002) 609–658.
[2] F. Chen, Industrial applications of low-temperature plasma physics, Phys. Plasmas 2 (1995) 2164–2175.
[3] J. Asmussen, Electron cyclotron resonance microwave discharges for etching and thin-film deposition, J. Vac. Sci. Technol. A 7 (1989) 883–893.
[4] J.P. Hopwood, Review of inductively coupled for plasma processing, Plasma Sources Sci. Technol. 1 (1992) 109–116.
[5] R. d'Agostino, Plasma Deposition, Treatment, and Etching of Polymers, Academic, New York, 1990.
[6] P. Geittner, D. Kuppers, H. Lydtin, Low-loss optical fibers prepared by plasma-activated chemical vapor deposition (CVD), Appl. Phys. Lett. 28 (1976) 645–646.
[7] H. Schlemm, A. Mai, S. Roth, D. Roth, K.M. Baumgartner, H. Muegge, Industrial large scale silicon nitride deposition on photovoltaic cells with linear microwave plasma sources, Surf. Coat. Technol. 174–175 (2003) 208–211 (Proceedings of the Eight International Conference on Plasma Surface Engineering).
[8] J. Feichtinger, A. Schulz, M. Walker, U. Schumacher, Sterilisation with low-pressure microwave plasmas, Surf. Coat. Technol. 174–175 (2003) 564–569.
[9] H. Lorentz, The absoption and emission lines of gaseous bodies, Proc. Amst. Acad. Sci. 8 (1906) 591–611.
[10] P. Kepple, H.R. Griem, Improved Stark profiles calculations for the hydrogen lines H_α, H_β, H_γ and H_δ, Phys. Rev. 173 (1968) 317–325.
[11] E.W. Smith, J. Cooper, C.R. Vidal, Unified classical-path treatment of Stark broadening plasmas, Phys. Rev. 185 (1969) 140–151.
[12] H.R. Griem, Spectral Line Broadening by Plasmas, Academic, New York, 1974.
[13] U. Frisch, A. Brissaud, Theory of Stark broadening soluble scalar model as a test, J. Quant. Spectrosc. Radiat. Transf. 11 (1971) 1753–1766.
[14] C. Sthelé, R. Hutcheon, Extensive tabulation of Stark broadened hydrogen line profiles, Astron. Astrophys. Suppl. Ser. 140 (1990) 93–97.
[15] M.A. Gigosos, V. Cardeñoso, New plasma diagnosis tables of hydrogen Stark broadening including ion dynamics, J. Phys. B: At. Mol. Opt. Phys. 29 (1996) 4795–4838.
[16] M.A. Gigosos, M.A. Gonzalez, V. Cardeñoso, Computer simulated Balmer-alpha, -beta and -gamma Stark line profiles for non-equilibrium plasmas diagnostics, Spectrochim. Acta Part B 58 (2003) 1489–1504.
[17] J. Torres, J. Jonkers, M.J. van de Sande, J.J.A.M. van der Mullen, A. Gamero, A. Sola, An easy way to determine simultaneously the electron density and temperature in high-pressure plasmas by using Stark broadening, J. Phys. D: Appl. Phys. 36 (2003) L55–L59.
[18] J. Torres, J.M. Palomares, A. Sola, J.J.A.M. van der Mullen, A. Gamero, A Stark broadening method to determine simultaneously the electron temperature and density in high-pressure microwave plasmas, J. Phys. D: Appl. Phys. 40 (2007) 5929–5936.
[19] H. Ehrich, D.E. Kelleher, Experimental investigation of plasma-broadened hydrogen Balmer lines at low electron densities, Phys. Rev. A 21 (1980) 319–334.
[20] C. Thomsen, V. Helbig, Determination of the electron density from the Stark broadening of Bahner Beta-comparison between experiment and theory, Spectrochim. Acta Part B 46 (1991) 1215–1225.
[21] E.W. Weber, R. Frankenberger, M. Schilling, Nonlinear plasma spectroscopy of the hydrogen Balmer-alpha line, Appl. Phys. B 32 (1983) 63–73.
[22] H. Hermann, J. Kruse, A. Piet, E.W. Weber, V. Helbig, Charged and neutral particle shift and broadening of resolved Balmer- beta fine structure lines at low electron densities, Plasma Sources Sci. Technol. 2 (1993) 214–218.
[23] J.P. Booth, J. Derouard, M. Fadlallah, L. Cabaret, J. Pinard, Electric field measurements in discharges by Doppler-free two-photon laser Stark spectroscopy of atomic hydrogen, Opt. Commun. 132 (1996) 363–370.
[24] M.A. Capelli, Q.E. Walker, P.V. Storm, Doppler-free absorption measurements of Stark broadening in a flowing hydrogen plasma, J. Quant. Spectrosc. Radiat. Transf. 66 (2000) 343–361.

[25] E. Ferguson, H. Schluter, Stark broadening of Balmer lines at low electron densities, Ann. Phys. 22 (1963) 351–372.
[26] Roger D. Bengtson, J.D. Tannich, P. Kepple, Comparison between measured and theoretical Stark-broadened profiles of H_6–H_{12} emitted from a low-density plasma, Phys. Rev. A 1 (1970) 532–533.
[27] E. Stambulchik, S. Alexiou, H.R. Greim, P.C. Kepple, Stark broadening of high principal quantum number hydrogen Balmer lines in low-density laboratory plasmas, Phys. Rev. E 75 (2007) 016401 (9 pp.).
[28] C.O. Laux, T.G. Spence, C.H. Kruger, R.N. Zare, Optical diagnostics of atmospheric pressure air plasmas, Plasma Sources Sci. Technol. 12 (2003) 125–138.
[29] Y. Kabouzi, M.D. Calzada, M. Moisan, K.C. Tran, C. Trassy, Radial contraction of microwave-sustained plasma columns at atmospheric pressure, J. Appl. Phys. 91 (2002) 1008–1019.
[30] Q. Wang, I. Koleva, V.M. Donnelly, D.J. Economou, Spatially resolved diagnostics of an atmospheric pressure direct current helium microplasma, J. Phys. D: Appl. Phys. 38 (2005) 1690–1697.
[31] X.M. Zhu, W.C. Chen, Y.K. Pu, Gas temperature, electron density and electron temperature measurement in a microwave excited microplasma, J. Phys. D: Appl. Phys. 41 (2008) 105212 (6 pp.).
[32] E. Tatarova, F.M. Dias, E. Felizardo, J. Henriques, C.M. Ferreira, B. Gordiets, Microwave plasma torches driven by surface waves, Plasma Sources Sci. Technol. 17 (2008) 024004 (7 pp.).
[33] S. Hofmann, A.F.H. van Gessel, T. Verreycken, P. Bruggeman, Power dissipation, gas temperatures and electron densities of cold atmospheric pressure helium and argon RF plasma jets, Plasma Sources Sci. Technol. 20 (2011) 065010 (12 pp.).
[34] N. de Vries, J.M. Palomares, E. Iordanova, E.M. van Veldhuizen, J.J.A.M. van der Mullen, Polydiagnostic calibration performed on a low pressure surface wave sustained argon plasma, J. Phys. D: Appl. Phys. 41 (2008) 205203–205212.
[35] M. Moisan, C. Beaudry, P. Leprince, A new HF device for the production of long plasma columns at a high electron density, Phys. Lett. 50A (1974) 125–126.
[36] M. Moisan, M. Chaker, Z. Zakrzewski, J. Paraszczak, The waveguide surfatron: a high power surface-wave launcher to sustain large-diameter dense plasma columns, J. Phys. E: Sci. Instrum. 20 (1987) 1356–1361.
[37] J.M. Palomares, E. Iordanova, E.M. van Veldhuizen, L. Baede, A. Gamero, A. Sola, J.J.A.M. van der Mullen, Thomson scattering on argon surfatron plasmas at intermediate pressures: axial profiles of the electron temperature and electron density, Spectrochim. Acta Part B 65 (2010) 225–233.
[38] Manual of the Double Echelle Monochromator (DEMON), Lasertechnik Berlin, http://www.ltb-berlin.de/Overview.122.0.html?&L=1, 2008 (last accessed).
[39] M.J. van de Sande, J.J.A.M. van der Mullen, Thomson scattering on a low-pressure, inductively-coupled gas discharge lamp, J. Phys. D: Appl. Phys. 35 (2002) 1381–1391.
[40] E. Iordanova, Poly-diagnostic validation of spectroscopic methods, in-depth monitoring of microwave induced plasmas. Ph.D Thesis, Eindhoven University of Technology, 2010.
[41] C.M. Ferreira, Modeling of a low-pressure plasma column sustained by a surface wave, J. Phys. D: Appl. Phys. 16 (1983) 167S–1685S.
[42] V.M. Lelevkin, D.K. Otorbaev, D.C. Schram, Physics of Non-equilibrium Plasmas 123, North-Holland, Elsevier Science Publishers B.V., 1992.
[43] A.W. Ali, H.R. Greim, Theory of resonance broadening of spectral lines by atom–atom impacts, Phys. Rev. 140 (1965) A1044–A1049.
[44] R. Konjevic, N. Konjevic, On the use of non-hydrogenic spectral line profiles for electron density diagnostics of inductively coupled plasmas, Spectrochim. Acta Part B 52 (1997) 2077–2084.
[45] C. Yubero, M.D. Calzada, M.C. Garcia, Using the Stark broadening of the H_α, H_β and H_γ lines for the measurement of electron density and temperature in a plasma at atmospheric pressure, J. Phys. Soc. Jpn. 74 (2005) 2249–2254.
[46] J. Torres, Estudio de técnicas de diagnosis y modelos en plasmas producidos por microondas a alta presión, Tesis Doctoral, Universidad de Córdoba, 2006.
[47] V. Helbig, Starkeffekt-verbreiterung von balmerlinien bei mittleren elektronendichten, Contrib. Plasma Phys. 31 (1991) 183–197.
[48] W. Olchawa, R. Olchawa, B. Grabowski, Stark broadening of hydrogen spectral lines with fine structure effects, Eur. Phys. J. D 28 (2004) 119–124.
[49] J. Seidel, R. Stamm, Effects of radiator motion on plasma-broadened hydrogen Lyman-β, J. Quant. Spectrosc. Radiat. Transf. 27 (1982) 499–503.
[50] R.G. Kulkarni, N.V.V.J. Swamy, E. Chaffin, First-order Stark shifts for low electric fields, Phys. Rev. A 7 (1973) 27–33.
[51] C. Stehle, Impact Stark broadening of the Lyman lines of hydrogenic ions under dense-plasma conditions: fine-structure effects, J. Phys. B: At. Mol. Phys. 18 (1985) L43–L48.
[52] M.A. Gonzalez, M.A. Gigosos, Tables of dipolar emission and two-photon absorption Lyman-α profiles, Astron. Astrophys. Suppl. Ser. 145 (2000) 491–494.
[53] http://physics.nist.gov/cgi-bin/ASD/lines1.pl, 2012 (last accessed).